Synthesis, Electronic and Optical Properties of Cobalt(II) Dithiocarbamate Fluorescent Nanowires for Optoelectronic Devices

Sanjeev K. Ujjain[1], Preety Ahuja[1], Raj K. Sharma[1] & Gurmeet Singh[1]

[1]Department of Chemistry, University of Delhi, Delhi-110007, India

Correspondence: Raj K. Sharma, Department of Chemistry, University of Delhi, Delhi-110007, India. E-mail: drrajksharma@yahoo.co.in; rajksharma@chemistry.du.ac.in

Abstract

Schiff base containing symmetric bis-dithiocarbamate ligand Na_2[dtc-SB-dtc] (SB = Bi-Schiff base Phenylene diamine) is synthesized and metallated with $Co(II)Cl_2.6H_2O$ to form $[Co(dtc-SB-dtc).2H_2O]_n$ Co(dtc-SB) infinite coordination polymer (ICP) nanowires [Co(dtc-SB) NWs]. Pair of Satellites in X-ray photoelectron spectroscopy (XPS) spectrum of Co 2p confirm the formation of hexa-coordinated Co(II). Presence of hyperfine pattern in low temperature EPR spectrum is due to the splitting of octahedral ground state $^4T_1$ for Co(II). Introduction of a rigid, non-planar, four membered dtc Cobalt chelating ring in coordination polymer assisted in reduction of photoinduced electron transfer (PET) process to yield high fluorescence. Prepared Co(dtc-SB) NWs are highly resistive however after suitable doping, exhibit p and n type conductivity. Temperature dependent conductivity results of different doping concentrations in NWs reflect activated type conduction with two different activation energies. UV-Visible absorption spectra show decrement in optical gap whereas emission spectra demonstrate quenching after p and n doping. Efficient quenching of emission indicates energy transfer between dopant ions and NWs.

Keywords: Cobalt(II) coordination polymer, Bis-dithiocarbamate Schiff base phenylenediamine (Na_2 [dtc-SB-dtc]), optical absorption & emission, conductivity

1. Introduction

Infinite Coordination polymers (ICPs) represent an area of growing interest in chemistry and materials science, owing to their potential application in drug delivery agent (Rieter, Pott, Taylor, & Lin, 2008), encapsulating matrices (Nishiyabu, Aime, Gondo, Noguchi, & Kimizuka, 2009), contrast agents (Taylor, Jin, & Lin, 2008), catalysis (Park, Jang, Son, & Sweigart, 2006), gas sorption (Tanaka et al., 2010), light harvesting (Zhang, Chen, & Loh, 2009), electronic and sensing devices (Coronado, Mascaros, Capilla, Martinez, & Pardo-Ibanez, 2007; Imaz et al., 2008; Rieter, Taylor, & Lin, 2007; Cho, Lee, Lee, & Oh, 2009). ICPs can be either highly crystalline structures, known as metal-organic frameworks (MOFs) (Oh, & Mirkin, 2005; Jeon, Heo, & Mirkin, 2007; Heo, Jeon, & Mirkin, 2007; Lu, Chui, Ng, & Che, 2008; Zhao et al., 2011) or amorphous nano/micro particles (Jeon, Armatas, Heo, Kanatzidis, & Mirkin, 2008). Metal ions in ICPs bridged with organic ligands establish coupling between conduction electrons (π electrons) and localized magnetic moments (d spins) through π–d interaction. These unique interactions give rise to multifunctional molecular materials with optical properties, electronic conductivity, magnetism and numerous others. Recently, a great attention is given to designed nanoscale ICPs with different morphologies such as spheres (Sun, Dong, & Wang, 2005; Champness, 2009; Imaz, Hernando, Molina, & Maspoch, 2009), cubes (Jung, & Oh, 2008), rods (Farha et al. 2009; Rieter, Taylor, An, Lin, & Lin, 2006), wheels (Lu, Chui, Ng, & Che, 2008) and nanofibres (Imaz, Mart ńez, Saletra, Amabilino, & Maspoch, 2009) as they can be easily dispersed in many solvents and exhibit size/shape dependent properties. In particular, nanoscale 0-D and 1-D ICPs, integrated with optical and electrical properties has potential applications in molecular optoelectronics. The tetrathiafulvalene (TTF) derivatives are mainly used for synthesizing conducting ICPs (Bryce, 1991). TTFs are organic π-electron donor compounds with organylthio groups as chelating sites (Bryce, 1995). Due to the tedious synthetic procedure and hazardous nature, TTFs could not be extended to practical applications (Mueller, & Ueba,1995). Developing new ligands with synthesis flexibility, low cost, three dimensional stacking capability along with excellent thermal stability and favourable physiochemical properties is a challenge.

Cookson (Cookson, & Beer, 2007) and Karlin (Karlin, & Hogarth, 2005) on the other hand, described dithiocarbamate (dtc) as an extremely versatile ligand for metal ion-directed self-assembly. In dtc, the enhanced overlap of sulphur p orbital with metal d and s orbitals results in high binding energy with reduced charge transfer barrier across the metal-molecule interface (Wrochem et al., 2010). Therefore dithiocarbamate (dtc) ligands if utilised, could serve as a building block for molecular electronics. Zaroma et al. and others (Mitsumi et al., 2001) have utilized alkyl dithiocarbamate (R-CS$_2$) ligand to synthesize conducting ICPs (Guijarro et al., 2010). Besides excellent conductivity, it lacks in optical properties simultaneously important for optoelectronic devices.

In this work, we report room temperature synthesis of Co(II) ICP nanowires (NWs) with dithiocarbamate ligand Na$_2$[dtc-SB-dtc] (SB = Bi-Schiff base Phenylene diamine). These Co(dtc-SB) NWs demonstrate tunable optical (absorption/emissions) properties and electronic conduction.

2. Experimental

2.1 Materials and Physical Measurements

Chemical reagents of AR grade were used for experimental work. Glyoxal (40% aqueous), Methanol, dimethyl formamide, p-Phenylenediamine, carbon disulphide, sodium hydroxide and cobalt salt (Co(II)Cl$_2$.6H$_2$O) were purchased from Merck. All solvents were distilled and kept with magnesium sulphate for several days to remove moisture. High Resolution Transmission electron microscopy (HRTEM) images, selected area electron diffraction patterns (SAED) and Energy-dispersive X-ray spectroscopy (EDX) results were obtained using transmission electron microscope (Philips Tecnai T-300). X-ray photoelectron spectrometer (XPS), Perkin-Elmer model 1257, was employed to study the chemical states, structure and composition of different elements present in the specimen. Fourier transform infrared (FTIR) spectra of ligand and complexes in KBr pellet were recorded using a Perkin-Elmer FT-IR spectrum BX spectrometer. Proton Nuclear Magnetic Resonance (^{1}H NMR) spectroscopy was performed at 25 ^{o}C using a Jeol ECX–400P, 400MHz spectrometer in DMSO- d_6. The Electron paramagnetic resonance (EPR) spectra were recorded at RT and 77 K on a JES - FA200 ESR Spectrometer at SAIF, IIT Bombay, India. UV-1601 Shimadzu UV-Vis spectrophotometer was used for recording the UV-Visible spectra of thin film of materials on glass substrate. Fluorescence measurement was conducted with a Cary Eclipse Spectrofluorimeter (Varian optical spectroscopy instruments, Mulgrave, Victoria, Australia). Elemental analysis was obtained from Elementer Analysensysteme GmbhVario E1-III instrument. TOF MS ES$^+$ spectra were recorded on MICROMASS (Waters) MODEL-KC 455. Thermogravimetric analysis (TGA) thermograms were recorded on RIGAKU, model 8150 Thermoanalyser (Thermaflex) in air flux. Conductivity measurement were carried out on metal complex pellet of known thickness and diameter (ca. 10 mm) using   two-point probe Keithley 2400, source meter. The powder sample was pressed at 200 kg cm^{-1}to form a pellet.

2.2 Synthesis

2.2.1 Synthesis of Ligand dtc-SB

Bis-dithiocarbamate Schiff base phenylenediamine ligand (dtc-SB) is synthesized with minor modification as reported (Gaur, Jain, Bhatia, Lal, & Kaushik, 2013). Synthesis of dtc-SB is a two step process.

2.2.1a. Synthesis of SB Ligand

p-Phenylenediamine was used as a precursor to synthesize Bi-Schiff base phenylenediamine (SB). This SB ligand was used to synthesize tetradentate bis-dithiocarbamate Schiff base phenylenediamine ligand (dtc-SB). 100 ml methanol (CH$_3$OH) solution of p-Phenylenediamine (60 mmol, 6.48g) was stirred for 30 minutes in an ice bath. Then 100 ml methanol solution of (40 wt. % in H$_2$O) glyoxal (30mmol, 1.74g) was added drop-wise to the homogenous solution and stirred for 75 minutes. Orange color precipitate formed. It was centrifuged and washed with CH$_3$OH and kept for drying overnight in vacuum desiccator. Yield: 6.44 g, (90 %). IR (solid state): υ(N-H)cm^{-1} 3412, 3320, 3218, υ(C=N)cm^{-1} 1607, υ(C-H out of-plane vibration) cm^{-1} 830.^{1}H NMR (DMSO-d_6): δ(ppm) = 6.3[s, 4H, NH$_2$], 6.59[d, 4H, ArH], 7.2[d, 4H, ArH], 8.35[s, 2H, H-C=N]. TOF MS ES$^+$: m/z = 238.52 [M$^+$] Anal: Calcd: C$_{14}$H$_{14}$N$_4$: C,70.57; H,5.92; N,23.51. Found: C,70.54; H,5.93; N,23.53.

2.2.1b. Synthesis of dtc-SB Ligand

1 mmol of SB (238 mg) and 2 mmol NaOH were dissolved in 100 ml of CH$_3$OH individually. These solutions were added dropwise in excessive CS$_2$ with constant stirring at 20 ^{o}C simultaneously. The solution was stirred for 2h. Pale yellow precipitate was formed, which was centrifuged and washed with CH$_3$OH and kept for drying overnight in vacuum desiccator. Yield: 0.316g, (72.6%). IR (solid state): υ(N-H)cm^{-1} 3385, 646, υ(H-C=N)cm^{-1} 2929, υ(C-H)cm^{-1} 2364 , υ(C=N)cm^{-1} 1605, υ(C=C) cm^{-1} 1507, υ(C-N)cm^{-1} 1216, υ(C ꞊꞊꞊ N)cm^{-1} 1390,

υ(S=C-S)cm^{-1} 1052,1004, υ(C-H out of-plane vibration)cm^{-1} 826. ^{1}H NMR (DMSO-d_6): δ(ppm) = 5.5[s, 2H, -NH], 6.59[d, 4H, ArH], 7.2[d, 4H, ArH], 8.35[s, 2H, H-C=N]. TOF MS ES$^+$: m/z = 436.01 [M$^+$+2H] Anal: Calcd: C$_{16}$H$_{12}$N$_4$Na$_2$S$_4$: C,44.22; H,2.78; N,12.89. Found: C,44.24 H,2.75; N,12.84.

2.2.2 Synthesis of [Co(dtc-SB).2H$_2$O]$_n$, (Co(dtc-SB)) Infinite Coordinated Polymer Nanowires

Bis-dithiocarbamate Schiff base phenylenediamine ligand (dtc-SB) (1 mmol, 436 mg) was dissolved in dimethyl formamide solution. To this solution, add cobalt(II) chloride hexahydrate (1 mmol, 237 mg). It was stirred for 3 to 4 h in dark. Brown colour precipitate formed after slow addition of pentene. It was centrifuged and washed with CH$_3$OH:DMF (9:1) mixture and was kept for drying over P$_2$O$_5$ in vacuum desiccator overnight. Yield: 402 mg , (76.30%). IR (solid state): υ(N-H)cm^{-1} 3310 (H-bonded), 634, υ(H-C=N)cm^{-1} 2962, υ(C-H)cm^{-1} 2360, υ(C=N)cm^{-1} 1600 (H-bonded), υ(C=C)cm^{-1} 1512, υ(C-N)cm^{-1} 1232, υ(C$=$N) cm^{-1} 1410, υ(S=C-S) cm^{-1} 1062, υ(C-H out of-plane vibration)cm^{-1} 826. TOF MS ES$^+$: m/z = 483 Anal: Calcd: C$_{16}$H$_{16}$N$_4$O$_2$S$_4$Co: C,39.74; H,3.34; N,11.59. Found: C, 39.62; H,3.29; N,11.67.

3. Results and Discussion

3.1 Synthesis

Synthesis of dtc-SB ligand and its cobalt complex (Co(dtc-SB)) is presented in Scheme 1. Schiff base Phenylenediamine ligand (SB) was first prepared using *p*-Phenylenediamine which get condensed with glyoxal to form imine bridged ligand SB. Direct introduction of aromatic rings in the ligand decreases the flexibility for structural change and consequently deactivate reactivity (Tabata, Tokoyama, Yamakado, & Okuno, 2012). In order to avoid any strain in the ligand conjugated system, aromatic rings are bridged using diimine to maintain the planarity. The SB ligand further reacts with CS$_2$ in presence of NaOH to form dtc-SB. So obtained pale yellow product was washed with CH$_3$OH/DMF (9:1:v/v) thrice and purity of the ligand was estimated using TLC and ^{1}H NMR spectroscopy. In all attempts, TLC analysis of the product shows single spot and its corresponding ^{1}H NMR spectrum (S1, ESI) indicates peaks corresponding to 4 different protons. Purified dtc-SB was further allowed to react with CoCl$_2$.6H$_2$O (1:1 molar) in DMF, followed by gradual pentane vapour diffusion to form Co(dtc-SB). Due to the diffusion of low polarity pentane, solubility of the complex decreased and aggregates were formed. HRTEM image (Fig. 1) shows that the Co(dtc-SB) forms well defined nanowires (NWs) (30 nm dia.). Selected area electron diffraction (SAED) pattern (inset Fig. 1b) in agreement with X-ray diffraction (not shown) results reveal the amorphous nature. 1D growth tendency is retained due to introduction of diimine maintaining high degree of planarity in the ligand. Consequently, it results in effective π-π interaction to form NWs.
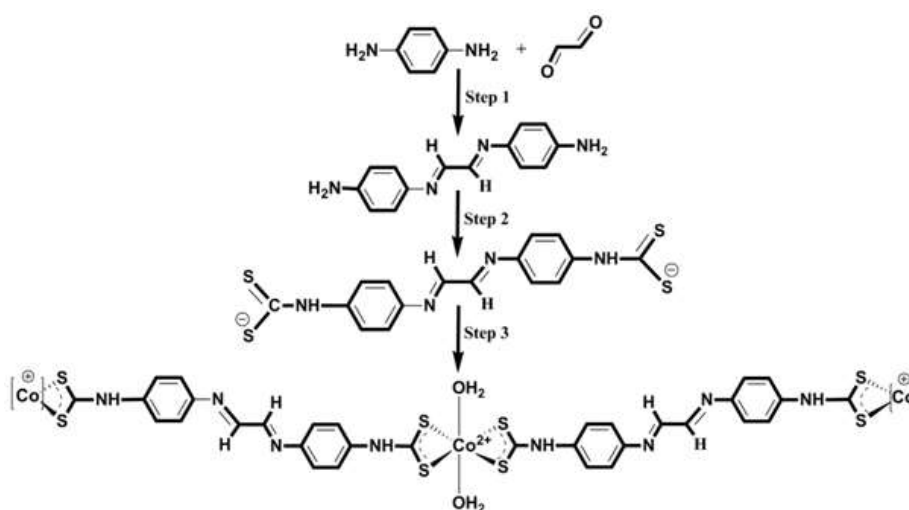
Scheme 1. Synthesis route of dtc-SB and Co(dtc-SB)   Step 1: CH$_3$OH, 0-5°C; Step 2: CH$_3$OH, NaOH, CS$_2$(excess), 20 ^{o}C;   Step 3: DMF, CoCl$_2$.6H$_2$O, RT.
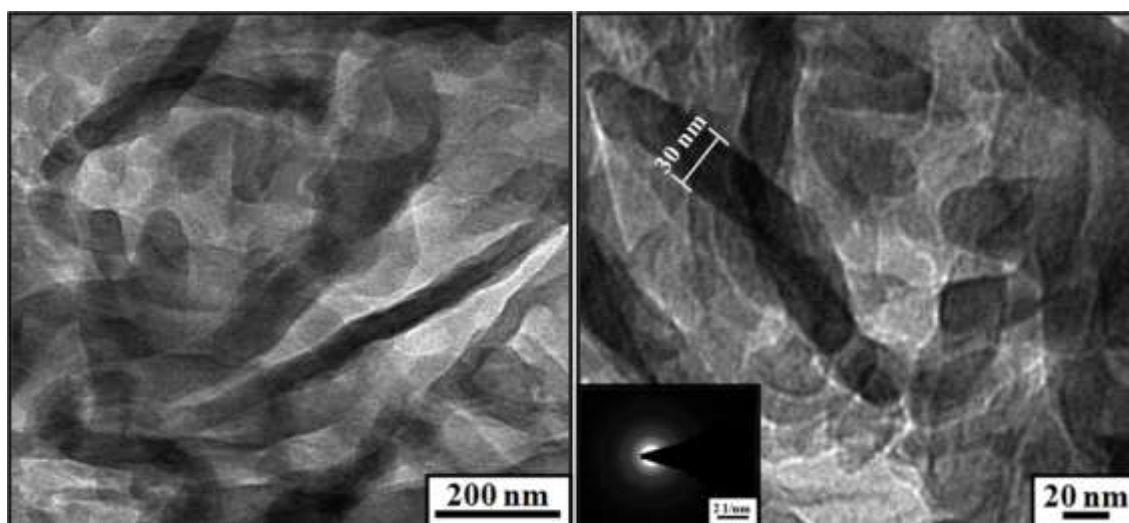
Figure 1. TEM images of (a) Co(dtc-SB) nanowires. (b) High resolution image, SAED (inset) show diffused rings pattern as a characteristics of amorphous nature.

3.2 Characterization

Co(dtc-SB) motif is particularly interesting, as Co(II) dithiocarbamate complexes are comparatively rare due to their high susceptibility towards oxidation (Karlin et al., 2005). Fabretti et al. and Harding et al. studied the role of substituent on electron donation ability of C⸺N and C⸺S bonds of dithiocarbamate ligands. They inferred that the benzyl substituted dithiocarbamate ligand could stabilize cobalt (II) complexes (Fabretti, Forghieri, Giusti, Preti, & Tosi, 1984; Harding, Harding, Dokmaisrijan, & Adams, 2011). This suggests that the synthesized dtc-SB ligand is vital to the successful synthesis of air stable Co(II) dithiocarbamate compounds. The Co(dtc-SB) NWs is highly resistive, so it is doped to generate mobile charges in π-electronic structure. These mobile charges are compensated by counter-ions which diffuse between the conjugated chains and Co(dtc-SB) exist as salts (Heeger, 2001). Iodine (I_2) and Sodium naphthalide in different concentrations are used as p and n-type dopant respectively (S2, ESI). When Co(dtc-SB) is exposed to iodine vapour, doping occurs through following chemical reaction.

$$3/2 \ xy(I_2) + [Co(dtc\text{-}SB)]_x \rightarrow [[Co(dtc\text{-}SB)]^{+y} (I_3^-)_y]_x \tag{1}$$
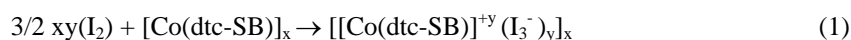
Here I_2 serves as oxidising agent and I_3^- as counter-ion.

During n-type doping, naphthalene$^-$ serves as the reducing agent and Na^+ is the counter ion.

$$y(Na^+)(naphtha^-) + [Co(dtc\text{-}SB)]_x \rightarrow [Na^{y+} [Co(dtc\text{-}SB)^{-y}]_x + (naphtha)_{neutral} \tag{2}$$

Elemental analysis of Co(dtc-SB) with and without doping is presented in Table S1, ESI. Iodine doping in Co(dtc-SB) is studied at low concentration i.e. 9.8 wt% I_2 and high as 20.2 wt%. Similarly, Sodium doping in Co(dtc-SB) is studied at 5.4 wt% and 11.53 wt%. Upon p and/or n doping, polymer structure remains intact and the partial oxidation involves orbitals which are largely of ligand in percentage (Diel et al., 1984).

Fig. 2 shows XPS spectra of the Co 2p, C 1s, N 1s, S 2p and O 1s. The spectrum of Co 2p exhibits complex satellite structure as shown in Fig. 2a. Binding energy difference (ΔE 15 eV) between Co $2p_{1/2}$ and Co $2p_{3/2}$ with pair of satellites support that Co(dtc-SB) is a hexa coordinated cobalt(II) complex (Atzei, Rossi, & Sadun, 2000; Baba, & Nakano, 2012; Battistoni, Gastaldi, Mattogno, Simeone, & Viticoli, 1987). Different peaks in C1s spectrum (Fig. 2b) are attributed to the chemically inequivalent carbons. The intensity of peaks depend on the tautomeric conformation adopted by the molecule. Peak at 287.6 eV is assigned to electron deficient carbon connected to the electronegative nitrogen atom (C=N) whereas, 286.2 eV peak shows two components C-N/C-S (Wohlgemuth, White, Willinger, Titirici, & Antonietti, 2012). The area under C-N/C-S peak is thrice of C=N peak, which is in agreement to the proposed molecular structure. The main carbon peak at 284.6 eV is assigned to benzene like carbon atoms (sp^2 C-C or C-H) (Wohlgemuth et al., 2012). XPS spectrum of N 1s (Fig.
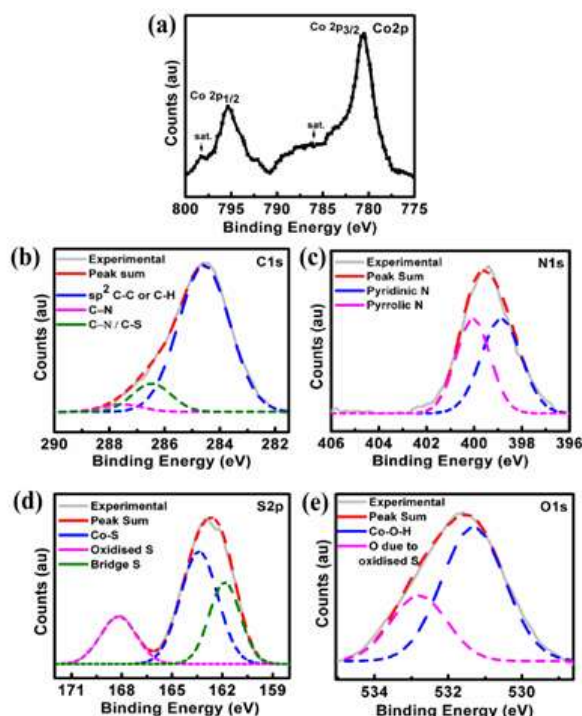
Figure 2. XPS Spectra of (a) hexa coordinated Co 2p. (b) C 1s. (c) N 1s. (d) S 2p and (e) O 1s.

Table 1. Binding Energy of different peaks in XPS spectra.

Peak	Binding energy(eV)	Assignment
Co 2p	780.4	$2p_{3/2}$
	795.3	$2p_{1/2}$
C 1s	284.6	Sp^2 C-C or C-H
	286.2	C-N / C-S
	287.6	C=N
N 1s	398.7	N1 pyridinic
	400.1	N2 pyrrolic
S 2p	161.8	Co-S-R
	162.9	Bridge S
	168.1	Oxidised S
O 1s	531.1	Co-O-H
	532.5	Due to oxidised S

2c) shows two peaks at 400.1 and 398.7 eV corresponding to the pyrrolic nitrogen and pyridinic nitrogen (Wohlgemuth et al., 2012) with an area ratio 1:1. Peaks in S 2p spectrum (Fig. 2d) at 161.8eV and 162.9 eV confirm the presence of cobalt bound sulphur (Co-S-R) and bridged sulphur (Atzei et al., 2000; Baba et al. 2012) respectively which is in close agreement with the molecular structure proposed by N. Giroud et al. for Zn and Mn dithiocarbamate complexes (Giroud, Dorge, & Trouve, 2010). Peak at 168.1 eV in S 2p spectrum originates from oxidised sulphur is correlated with the peak at 532.5eV of O 1s spectra in Fig. 2e. This oxidised sulphur peak could be due to the absorbed oxygen in Co(dtc-SB) NWs (Yang, Sun, Guo, & Da, 1999). Peak at 531.1eV in O 1s indicates the presence of Co-O-H in the structure (Atzei et al., 2000; Baba et al. 2012). Different peaks assigned in the spectra along with their binding energies are shown in Table 1. This confirms that the above results are in correlation with proposed Co(dtc-SB) structure, where each Co(II) hexa coordinated metal centre possess two dithiocarbamate ligand in bidentate mode and two H_2O molecule in axial positions. Further investigation on different functionalities present in the ligand structure and the change in electronic states upon complexation and doping are analyzed using FTIR. Stretching vibrations at 1052cm^{-1} (CS$_{2asymmetric\ stretching}$), 1004cm^{-1} (CS$_{2symmetric\ stretching}$), 1390cm^{-1} (C----N stretching) and 1605cm^{-1} (C=N stretching) of the dtc-SB in FTIR spectrum (Fig. 3a) confirms the presence of the dithiocarbamate and imine moieties (Gaur et al., 2013).

Peaks at 3385 cm^{-1} and 646 cm^{-1} correspond to anti-symmetric and rocking stretching vibration of N-H (Pavia, Lampman, Kriz, & Vyvyan, 2007; Kross, Fassel, & Margoshes, 1956) (Fig. S3, ESI). FTIR results show that the characteristic absorption of dtc-SB at 1004 cm^{-1}($CS_{2symmetric\ stretching}$) disappeared after the complex formation with cobalt (Fig. 3b). Major (ca. 10 & 20 cm^{-1}) shift in wave number of the characteristic absorption peak for anti-symmetric stretching vibration of CS_2 at 1052 cm^{-1} and S_2C=N stretching vibration at 1390 cm^{-1} support the complexation of Cobalt with dithiocarbamate moiety resulting in linear chain structure. Change in electronic structure of I_2 doped and Na doped Co(dtc-SB) (Fig. 3 c & d) is attributed to formation of charge transfer complex between dopant and the conjugated system (Dai, 1992). Broad peaks at 1605 and 1486 cm^{-1} in the IR spectrum of I_2 doped Co(dtc-SB) and peaks at 1597 and 1458 cm^{-1} for Na doped Co(dtc-SB) are characteristic of nitrogen quinoid   and benzenoid structure. Their presence strongly support the conducting state of conjugated system (Collman et al., 1986 & Dhawan, & Trivedi, 1992). The broadening of electronic absorptions on going from undoped to the doped Co(dtc-SB) is credited to the low electronic transitions. This is often found as a signature of highly conductive materials and are thought to result from either inter or intra valence band transition (Dhawan et al., 1992). Moreover, the desired formation of ligand and its complex Co(dtc-SB) is also confirmed by ^{1}H-NMR and X-band EPR respectively.   The ^{1}H NMR of dtc-SB shows resonance signals corresponding to 4 different protons in different electronic environment. The broad peak for N-H protons appears at δ 5.5 ppm whereas aromatic protons appear at δ 6.5 ppm and δ 7.2 ppm   respectively (Kross et al., 1956; West, Stark, Bain, & Leberta, 1996). The higher denomination of δ 8.3 ppm is assigned to imine protons (S1, ESI) (Gaur et al., 2013). First-derivative X-band EPR spectra of powdered Co(dtc-SB) NWs is recorded at room temperature (RT) and liquid N_2 (77 K) to analyse the coordination geometry around the Co ion. The X-band spectra are not well-resolved at RT, however an orthorhombic spectrum with hyperfine splitting pattern of high-spin Co^{2+} in octahedral sites is observed at 77 K (Fiorani, Gastaldi, & Viticoli, 1983) (Fig. 4). Furthermore, very short spin-lattice relaxation time and strong anisotropy of the g factor percluding hyperfine splitting of EPR
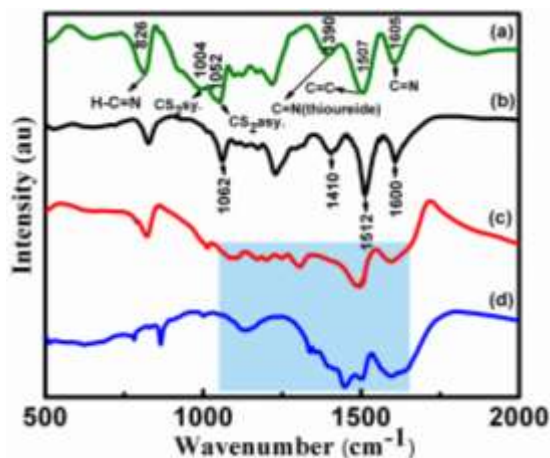

Figure 3. FTIR spectra of (a) ligand dtc-SB. (b) Cobalt complex Co(dtc-SB). (c) I_2 (p) doped Co(dtc-SB) and (d) Na (n) doped Co(dtc-SB). The peaks of IR spectrum are described in the order they appeared in the structures (See Scheme 1).

signal are characteristics of Co(II) ions in octahedral sites . At LNT, the observed spectra for Co(dtc-SB) complex can be described in terms   of a spin doublet S' = 1/2 that arises from the splitting of the octahedral ground state $^4T_1$ for Co^{2+} ions by the low-symmetry field and spin-orbit coupling (Fiorani et al., 1983; Nunez et al., 2011). The calculated EPR parameters, g_{II} = 2.168 & $g_{\perp}$ = 2.077 are consistant with those found for Co^{2+} ions in octahedral geometry [44]. In addition, the TOF MS ES$^+$ indicates the presence of the bridging ligand dtc-SB at m/z 388.6 which supports the imine bridged dithiocarbamate ligand remains intact in the polymer backbone. Chemical composition of Co(dtc-SB) NWs using Elemental analysis and energy dispersed X-ray (EDX) spectroscopy (S4, ESI) further support the presence of cobalt, carbon, nitrogen and sulphur in 1:1 cobalt–ligand complex. Further quantification was done by thermal analysis. dtc-SB differs significantly in thermal properties from its cobalt complex. Most striking difference is the char residue which in case of Co(dtc-SB) is about 15% whereas negligible char residue is obtained from dtc-SB. The char residue of Na doped Co(dtc-SB) is ~22%, while in case of I_2 doping this reduces to 17% (Fig. 5). TG thermogram of dtc-SB shows three decomposition steps. The first decomposition due to dehydration occurs between 50-200 °C with ~10% mass loss. Subsequent mass loss (~35%) between 200 and 480 °C is attributed to the breakdown of dithiocarbamate

moiety (Raja, Bhuvanesh, & Natarajan, 2012). The third and final mass loss between 490 °C to 780 °C occurs due to decomposition of the organic part of the ligand (Giovagnini et al., 2008). Co(dtc-SB) also follows the similar three stage degradation trend as observed for dtc-SB however shows better stability. Two molecules of H_2O as calculated from the percentage mass loss has been dehydrated at 200 °C. The char residue may be Co oxide. The TGA curves of Co(dtc-SB) confirm that the thermal stability of dtc-SB is enhanced on complexation with Co. I_2 doped Co(dtc-SB) decomposes sharply at about 135 °C due to the elimination of free I_2 (Giovagnini et al., 2008). However, there is no considerable change in the TG behaviour after Na doping in Co(dtc-SB).
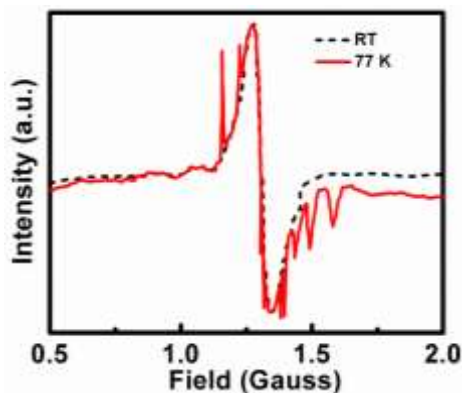

Figure 4. EPR spectra of Cobalt complex Co(dtc-SB) at room temperature and liquid N_2 (77 K).
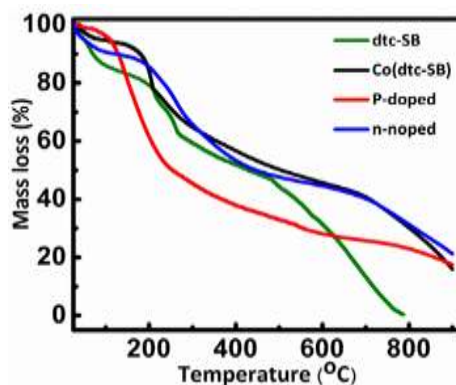

Figure 5. TGA thermograms of synthesized ligand dtc-SB; its cobalt complex Co(dtc-SB); I_2 (p) doped Co(dtc-SB) and Na (n) doped Co(dtc-SB).

3.3 Optical Properties of Co(dtc-SB) NWs

Co(dtc-SB) is a brown powder with yellowish tinge in solution. In order to examine the optical properties of Co(dtc-SB) NWs, optical absorption of thin film and optical emission spectra in DMSO solution was recorded (Fig. 6). The extent of conjugation in a conjugated system directly affects the observed energy of π-π* transitions i.e. the maximum absorption (λ_{max}). Quantitative comparison of thin film UV-Vis spectra of neutral and doped Co(dtc-SB) show change in absorption due to different π-π* transitions. These transitions occur between the charge transfer complex formed between dopant and conjugated system. Absorption edge of doped and undoped Co(dtc-SB) extends about 590-685 nm, from which the optical band gap energy difference (E_g) is calculated using the Tauc equation: $(\alpha h\nu)^n = K(h\nu - E_g)$. The plot of $(\alpha h\nu)^2$ vs. $h\nu$ is plotted and E_g is determined from the extrapolated intercept on the energy ($h\nu$) axis (Inset Fig. 6 a). The E_g of the Co(dtc-SB) is estimated to be 2.1 eV and for that of Na and I_2 doped Co(dtc-SB) is 2.04 eV and 1.8 eV respectively. Fig. 6b shows the photograph of the Co(dtc-SB) (undoped & doped) DMSO solution (1mg/ml), which was utilized to study its emission spectroscopy, as discussed in the next section.

Fluorescence emission spectra of the Co(dtc-SB) NWs with and without doping in DMSO solution (1μg/ml) was investigated. dtc-SB does not show any noticeable fluorescence upon excitation at 380 nm whereas Co(dtc-SB) and its doped derivatives display very strong fluorescence extended to about 455-526 nm with stokes shift of ~75 nm to 146 nm, shown in Fig. 6c. This implies that emission behaviour arises as a result of ligand-metal charge

transfer (LMCT). The I_2 doped Co(dtc-SB) displays fluorescence emission with stokes shift of 146 nm whereas the Na doped sample exhibits 86 nm stokes shift. High fluorescent behaviour in Co(dtc-SB) NWs is attributed to the complex formation leading to reduction of PET process (Sreedaran et al., 2008). Four membered chelate ring present in Co(dtc-SB) increases rigidity in comparison to free ligand, which in turn, reduces the loss of energy by vibrational decay and enhances the fluorescence intensity (Pandey et al., 2011). The efficient quenching of the emission intensity on I_2 and Na doping suggests the effective energy transfer from dopant ions to NWs, which is also seen in FTIR results (Peng, Xiao, Ma, Yang, & Yao, 2005). Efficient energy transfer is reflected in multifold increase in conductivity of doped samples. Fluorescence emission behaviour of the Co(dtc-SB) NWs is comparable to that of other fluorescent supramolecular polymeric nanowires (Luo et al., 2009). Remarkably, the high fluorescence behaviour of complexes is confirmed in acetonitrile and found that it produced measurable signal even in nanomolar (nm) range.
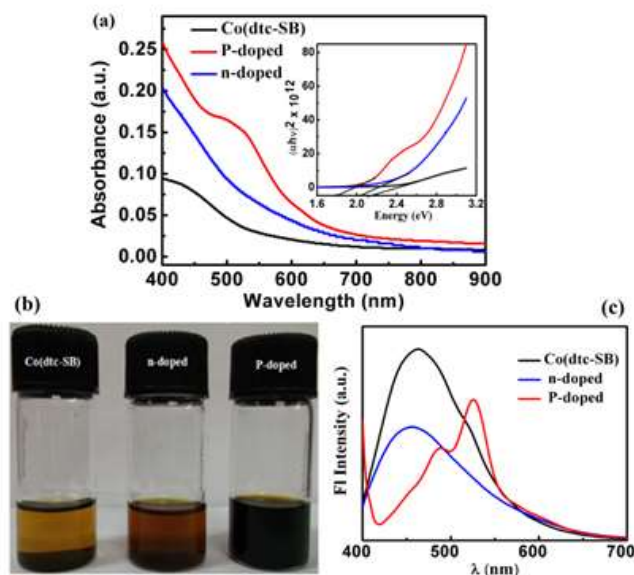

Figure 6. (a) Uv-vis absorption spectrum of Co(dtc-SB), I_2 doped Co(dtc-SB)and Na doped Co(dtc-SB) thin film : Inset graph shows a plot of hv versus $(ahv)^2$ of Co(dtc-SB)and its doped derivatives. (b) Estimated optical band gap commensurate with the color of samples in DMSO solution. (c) Fluorescence spectra of Co(dtc-SB) and its doped derivatives. λ_{ex} = 380 nm, λ_{em}= 455-526 nm, slit width (5 nm/5 nm , 500 V PMT).

3.4 Conductivity Study

Fig. 7a shows the current-voltage (I-V) characteristics of low concentration (9.8%) I_2 doped Co(dtc-SB) NWs between 300-425 K. I-V curves are linear in -5 to 5 V voltage range confirming ohmic behaviour. Current in the I_2 doped Co(dtc-SB) NWs is increased by two order of magnitude, when temperature is raised from 300 K to 425 K. Resistance (R) calculated from the slope of the curve is ~ 28 Mohm at 300 K, which gradually decreases to ~ 300 kohm on increasing temperature (425 K).   I-V plots of the high (20.2%) I_2 doped Co(dtc-SB) NWs in 300-400 K temperature range (Fig. 7b) show linear trend only in the range of -1 to 1 V. Above this range I-V characteristics deviates from the linear trend but they remain symmetric. The resistance (R) of the high I_2 doped Co(dtc-SB) NWs is found to be 60 kohm at 300 K which decreases to 7 kohm at 400 K. The high I_2 doped sample is more conducting (by 3 orders of magnitude) compared to low doped sample. TG analysis shows that material degrades above this temperature and this fact is also reflected in I-V curve which exhibits increase in *R* above 400 K. Non-linearity in high doped I_2 Co(dtc-SB) NWs may be due to scattering between the Co and I_2 or I_2-I_2 atoms. High doping concentration of I_2 induces additional disorder and hopping centres and the effect becomes prominent (Zakirov et al., 2011).

To study n-type conduction, Co(dtc-SB) NWs were doped with Na-naphthalide. I-V curve for low (5.4%) Na doped Co(dtc-SB) NWs shows an entirely different behaviour from p type doping (Fig. 7c). I-V characteristics are asymmetric and show rectification in positive voltage regime. At +ve low voltage (< 1volts) the I-V curve is linear and the R of the sample is found to be ~ 3 Mohm. Upon increasing the Na doping level to 11.5%, I-V curve becomes more symmetric as shown in Fig. 7d. We also noticed that current does not falls to ~ 0 at 0 voltage because of hysteresis observed in polymeric material (Hwang, Oh, Hwang, Kim, & Im, 2008).

Fig. 8 shows the R vs 1/T plot for doped complexes in semi logarithmic scale. Inset of Fig. 8a is R vs T plot for low I_2 doped Co(dtc-SB) NWs. The R of the sample is 28 Mohm which decreases to 300 kohm with increase in temperature to 425 K indicate semiconducting behaviour. Consequently, conductivity increased from 2.2E-8 to 1.4E-5 Scm^{-1}. In order to ascertain the conduction mechanism, log R vs 1/T plotted in Fig. 8a show two different slopes. This kind of behaviour is reported earlier in doped polymeric sample (Tabata et al, 2012). This plot is linear with two different slopes, implicating two different activated conduction in low I_2 doped Co(dtc-SB) NWs. The slope of the curve near 300K is higher compared to slope at 425 K region. A similar behaviour is observed in high I_2 doped sample. The R of the sample at room temperature is observed to be ~ 60 kohm (σ ~ 1.4E-5 Scm^{-1}) which decreases to 7 kohm (σ ~ 0.12 mScm^{-1}) at 400 K. The decrease in resistance is attributed to high level doping (Guijarro et al, 2010; Heeger, 2001). Fig. c inset shows the R-T behaviour for n-doped (Na) Co(dtc-SB) NWs which is apparently similar to p-doped sample. The resistance is 3 Mohm at 300 K which is decreased to 200 kohm at 430 K. The log R vs 1/T plot exhibits two different slopes analogous to I_2 doped Co(dtc-SB) NWs. In this case, the slope near to the room temperature is less
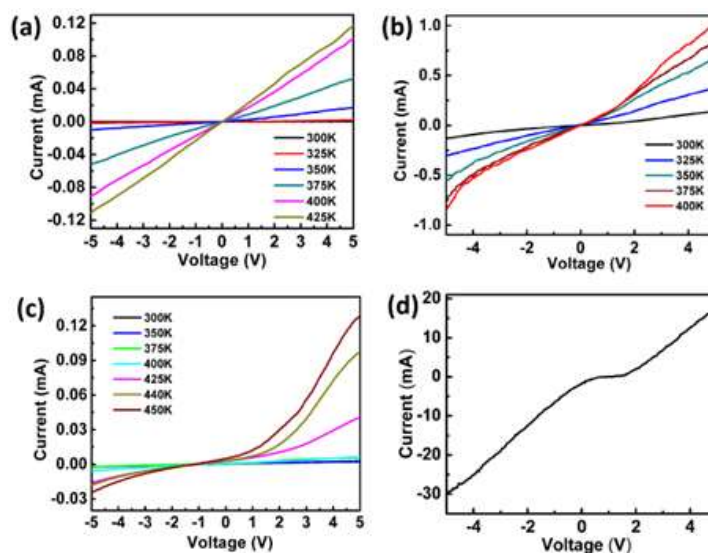

Figure 7. Current-Voltage curve of I_2 and Na doped Cobalt complex: (a) Low I_2 doped (9.8 wt.%) Co(dtc-SB) shows linear response.(b) At high I_2 doping (20.2 wt.%) I-V response becomes non-linear. (c)   Co(dtc-SB) doped with Na (5.4 wt.%) shows asymmetric I-V response. (d) At higher Na doping (11.5 wt.%) the charge blockade is observed at low voltages.
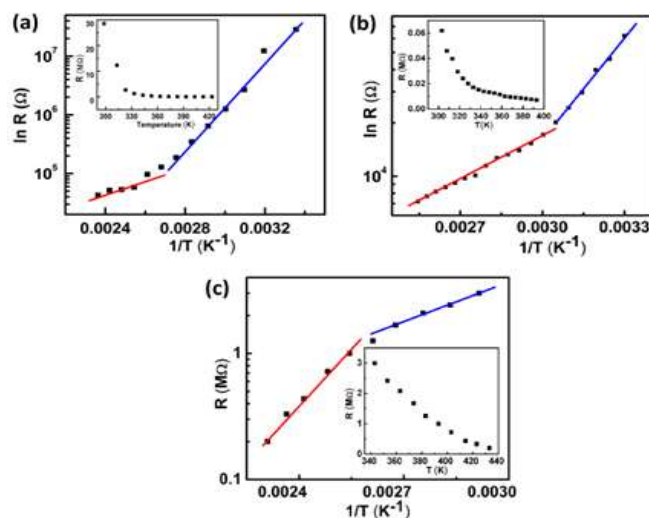

Figure 8. Plots of ln R vs 1/T. Inset shows R-T curve for I_2 and Na doped Co(dtc-SB): (a) Low I_2 doped complex, two different slopes are observed. (b) High I_2 doping shows similar behaviour. (c)   Low Na doped complex also two different slopes are observed.

steep compared to slope at high temperature. Doped Co(dtc-SB) NWs indicate a conduction mechanism by the combination of two activated conductions $\rho (T) = \rho_1 \exp(E_1/kT)$ and $\rho (T) = \rho_2 \exp(E_2/kT)$ with varying activation energies E_1 and E_2. The activation energy is calculated from the slope of the lnR vs 1/T plot. For room temperature regime, the activation energy for low I_2 doped Co(dtc-SB) NWs is 680 meV which decreases to 140 meV at high temperatures. Slope of the conductivity changes widely depending upon the dopant concentration, microstructure of the sample and backbone of the structure. We hypothesize that the doping with I_2 or Na creates a dopant level which is responsible for second activation. The activated transport due to doping is multistep hopping mechanism where charge hops along ligand backbone as illustrated in Fig. 9.
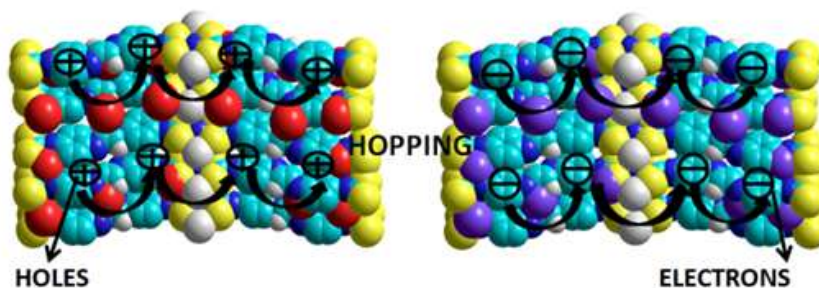

Figure 9. Schematic illustration of the hopping process in (a) Hole conduction in Iodine (I_3^-/I_5^-) (red balls) doped Co(dtc-SB) and (b) Electronic conduction in Sodium (purple balls) doped Co(dtc-SB).

A lower activation energy 370 meV is observed in room temperature regime for high I_2 doped Co(dtc-SB) NWs which is expected. In high temperature regime, the activation energy for high I_2 doped sample (160 meV) is approximately same as for low I_2 doped sample. It is evident from these observations that the activation energy in room temperature regime appears due to dopant ions. At high doping level, we observed relatively lower activation energy. As the temperature is increased, complex itself started contributing in conduction. Both low doped and high I_2 doped samples exhibit nearly same activation energy. At elevated temperature, polymer itself contributes in charge conduction due to onset of molecular motion. The Na doped Co(dtc-SB) NWs exhibits similar behavior. The activation energy in room temperature regime is 590 meV which decreases to 210 meV at high temperature. As evident from the I-V characteristics, I_2 doped Co(dtc-SB) NWs exhibit ohmic behaviour whereas I-V characteristics of Na doped Co(dtc-SB) NWs showed asymmetry and rectification. This difference in electrical properties arises from the dopant size (Bantikassegn, & Inganas, 1996). This small ion discrimination occurs in spite of the fact that these Co(dtc-SB) NWs are amorphous and do not possess well-defined channels as observed in crystalline metal-organic frameworks(MOFs). This implies that although NWs are amorphous, there must be some disordered pore structure as evident in metallo-salen ligand Zn(AFSL) amorphous ICP particles (Nishiyabu et al., 2009). Small Na^+ ion moves into and out of such disordered pores in nanowires matrix during oxidation/reduction cycles. This gives rise to rectification behaviour while no such detectable difference occurs in the sample having I_3^- as counter ions. In summary of these results, it can be concluded that small ions are easily transported through ICP pores, while the polymeric anions I_3^- are not at all mobile. This may be attributed for the major difference in I-V characteristics observed. This leads to the foundation of the proposed mechanism for charge transport in doped ICPs. However, further investigation is necessary to verify the mechanism.

4. Conclusion

A diimine containing dithiocarbamate ligand (dtc-SB) is synthesized by a simple and effective condensation process and utilized as building block for multi-functional coordination polymer nanowires by precipitation/coordination polymerization to form Co(dtc-SB) NWs. Structural analysis confirm that nanowires are formed by uniform π-π stacking of Co(dtc-SB). Presence of pair of satellites in Co 2p XPS spectrum and the binding energy difference (ΔE) of 15 eV between Co $2p_{1/2}$ and Co $2p_{3/2}$ indicate the presence of hexa coordinated Co(II) in Co(dtc-SB) NWs. Furthermore, hyperfine splitting pattern and 'g' parameters in liquid N_2 EPR spectrum confirms high spin octahedral coordination environment of Co^{2+} with two dithiocarbamate ligands coordinated in bidentate mode and axial positions are occupied by two H_2O molecules in cis configuration. The Co(dtc-SB) NWs show decrement in optical band gap when doped with iodine and sodium. They are fluorescent and show stoke shift of 75 nm when excited at 380 nm while I_2 and Na doped sample show stoke shift of 146 and 86 nm respectively. The remarkable change in stoke shift and efficient quenching of emission in doped samples may be attributed to the efficient energy transfer from polymeric iodine dopant (I_3^-/I_5^-)/Na^+ to

the nanowires. Electrical characterisation of Na/I_2 doped Co(dtc-SB) NWs show conductivity of the order of 3 mS/cm. The conductivity of the doped nanowires follow doubly activated behaviour with continuous increase with increasing temperature confirming their semiconducting nature. Therefore, these bi-functional Co(dtc-SB) NWs will create potentially versatile platform for generating electronic and photoactive devices.

Acknowledgements

References

Atzei, D., Rossi, A., & Sadun, C. (2000). Synthesis and characterization of a cobalt(III) complex with 1-(D-3-mercapto-2-methylpropionyl)-L-proline *Spectrochim. Acta A, 56,* 1875-1886. http://dx.doi.org/10.1016/S1386-1425(00)00246-8

Baba, H., & Nakano, M. (2012). Magnetic and spectroscopic characterizations of high-spin cobalt(II) complex with soft-scorpionate ligand. *Inorganic Chemistry Communications, 17,* 177-179. http://dx.doi.org/10.1016/j.inoche.2012.01.003

Bantikassegn, W., & Inganas, O. (1996). The electrical properties of junctions between aluminium and doped polypyrrole. *Journal of Physics D: Applied Physics, 29,* 2971-2975. http://dx.doi.org/10.1088/0022-3727/29/12/005

Battistoni, C., Gastaldi, L., Mattogno, G., Simeone, M.G., & Viticoli, S. (1987). Structural and magnetic properties of layer compounds: $CoGaInS_4$. *Solid State Communications, 61,* 43-46. http://dx.doi.org/10.1016/0038-1098(87)90011-1

Bryce, M. R. (1991). Recent progress on conducting organic charge-transfer salts. *Chemical Society Review, 20,* 355-390. http://dx.doi.org/10.1039/CS9912000355

Bryce, M. R. (1995). Current trends in tetrathiafulvalene chemistry: towards increased dimensionality. *Journal of Material Chemistry, 5,* 1481-1496. http://dx.doi.org/10.1039/JM 9950501481

Champness, N. R. (2009). Coordination Polymers: From Metal–Organic Frameworks to Spheres. *Angewandte Chemie International Edition*, 48, 2274-2275. http://dx.doi.org/10.1002/anie. 200806069

Cho, W., Lee, Y. J., Lee, H. J., & Oh, M. (2009). Systematic transformation of coordination polymer particles to hollow and non-hollow In_2O_3 with pre-defined morphology. *Chemical Communication,* 4756-4758. http://dx.doi.org/10.1039/ B907281K

Collman, J. P., McDevitt, J. T., Yee, G. T., Leidner, C. R., McCullough, L. G., Little, W. A., & Torrance, J. B. (1986). Conductive polymers derived from iron, ruthenium, and osmium metalloporphyrins: The shish-kebab approach. *PNAS Proceedings of the National Academy of Sciences, 83,* 4581-4585. http://www.pnas.org/ content/83/13/4581.short

Cookson, J., & Beer, P. D. (2007). Exploiting the dithiocarbamate ligand in metal- directed self-assembly. *Dalton Transactions,* 1459-1472. http://dx.doi.org/10.1039/ B618088D

Coronado, E., Mascaros, J. R. G., Capilla, M. M., Martinez, J. G., & Pardo-Ibanez, P. (2007). Bistable Spin-Crossover Nanoparticles Showing Magnetic Thermal Hysteresis near Room Temperature. *Advanced Materials, 19,* 1359-1361. http://dx.doi.org/ 10.1002/adma.200700559

Dai, L. (1992). Charge-transfer complexes between polyacetylene-type polymers and iodine in solution. *Journal of Physical Chemistry, 96*, 6469-6471. http://dx.doi.org/10.1021/ j100194a067

Dhawan, S. K., & Trivedi, D. C. (1992). Synthesis and properties of polyaniline obtained using sulphamic acid. *Journal of Applied Electrochemistry, 22,* 563-570. http://dx.doi.org/10.1007/BF01024098

Diel, B. N., Inabe, T., Jaggi, N. K., Lyding, J. W., Schneider, O., Hanack, M., Kannewurf, C. R., Marks, T. J., & Schwartz, L. H. (1984). Cofacial assembly of metallomacrocycles as an approach to controlling lattice architecture in low-dimensional molecular solids. Chemical, structural, oxidation-state, transport, and optical properties of the iron coordination polymer [Fe(phthalocyaninato)(.mu.-pyrazine)]n and the consequences of halogen doping. *Journal of the American Chemical Society, 106,* 3207-3214. http://dx.doi.org/10.1021/ja00323a024

Fabretti, A. C., Forghieri, F., Giusti, A., Preti, C., & Tosi, G. (1984). The syntheses and properties of cobalt(II), nickel(II) and copper(II) complexes with some heterocyclic dithiocarbamates. *Inorganica Chimica Acta, 86,* 127-131. http://dx.doi.org/10.1016/S0020-1693(00)82333-6

Farha, O. K., Spokoyny, A. M., Mulfort, K. L., Hupp, J. T., Galli, S. & Mirkin, C. A. (2009). Gas-Sorption Properties of Cobalt(II)–Carborane-Based Coordination Polymers as a Function of Morphology. *Small, 5,* 1727-1731. http://dx.doi.org/ 10.1002/smll.200900085

Fiorani, D., Gastaldi, L., & Viticoli, S. (1983). X-ray and spectroscopic investigations on polycrystalline $Co_xZn_{1-x}In_2S_4$ solid solution. *Solid State Communications, 48,* 865-867. http://dx.doi.org/10.1016/0038-1098(83)90135-7

Gaur, J., Jain, S., Bhatia, R., Lal, A., & Kaushik, N. K. (2013). Synthesis and characterization of a novel copolymer of glyoxal dihydrazone and glyoxal dihydrazone bis(dithiocarbamate) and application in heavy metal ion removal from water. *Journal of Thermal Analysis and Calorimetry, 112,* 1137-1143. http://dx.doi.org/10.1007/s10973-013-3136-x

Giovagnini, L., Sitran, S., Montopoli, M., Caparrotta, L., Corsini, M., Rosani, C., Zanello, P., Dou, Q. P., & Fregona, D. (2008). Chemical and Biological Profiles of Novel Copper(II) Complexes Containing S-Donor Ligands for the Treatment of Cancer. *Inorganic Chemistry, 47,* 6336-6343. http://dx.doi.org/10.1021/ic800404e

Giroud, N., Dorge, S., & Trouve, G. (2010). Mechanism of thermal decomposition of a pesticide for safety concerns: Case of Mancozeb. *Journal of Hazardous Materials, 184,* 6-15. http://dx.doi.org/10.1016/j.jhazmat.2010.07.053

Guijarro, A., Castillo, O., Welte, L., Calzolari, A., Sanz Miguel, P. J., Gomez-Garcia, C. J., Olea, D., Felice, R. di., Gomez-Herrero, J., & Zamora, F. (2010). Conductive Nanostructures of MMX Chains. *Advanced Functional Materials, 20,* 1451-1457. http://dx.doi.org/ 10.1002/adfm. 200901901

Harding, D. J., Harding, P., Dokmaisrijan, S., & Adams, H. (2011). Redox-active nickel and cobalt tris(pyrazolyl)borate dithiocarbamatecomplexes: air-stable Co(II) dithiocarbamates. *Dalton Transactions, 40,* 1313-1321. http://dx.doi.org/10.1039/ C0DT01010C

Heeger, A. J. (2001). Semiconducting and Metallic Polymers: The Fourth Generation of Polymeric Materials (Nobel Lecture). *Angewandte Chemie International Edition, 40,* 2591-2611. http://dx.doi.org/10.1002/1521-3773(20010716)40:14<2591:: AID-ANIE2591> 3.0.CO;2-0

Heo, J., Jeon, Y. M., & Mirkin, C. A. (2007). Reversible Interconversion of Homochiral Triangular Macrocycles and Helical Coordination Polymers. *Journal of the American Chemical Society, 129,* 7712-7713. http://dx.doi.org/10.1021/ja0716812

Hwang, D. K., Oh, M. S., Hwang, J. M., Kim, J. H., & Im, S. (2008). Hysteresis mechanisms of pentacene thin-film transistors with polymer/oxide bilayer gate dielectrics. *Applied Physics Letters, 92,* 013304(1-3). http://dx.doi.org/10.1063/ 1.2830329

Imaz, I., Hernando, J., Molina, D. R., & Maspoch, D. (2009). Metal–Organic Spheres as Functional Systems for Guest Encapsulation. *Angewandte Chemie International Edition, 48,* 2325-2329. http://dx.doi.org/10.1002/anie. 200804255

Imaz, I., Mart ńez, M. R., Saletra, W. J., Amabilino, D. B., & Maspoch, D. (2009). Amino Acid Based Metal−Organic Nanofibers. *Journal of the American Chemical Society, 131,* 18222-18223. http://dx.doi.org/10.1021/ja908721t

Imaz, I., Maspoch, D., Blanco, C. R., Falcon, P. M. J., Campo, J., & Molina, D. R. (2008). Valence-Tautomeric Metal–Organic Nanoparticles. *Angewandte Chemie International Edition, 47,* 1857-1860. http://dx.doi.org/10.1002/anie.200705263

Jeon, Y. M., Armatas, G. S., Heo, J., Kanatzidis, M. G., & Mirkin, C. A. (2008). Amorphous Infinite Coordination Polymer Microparticles: A New Class of Selective Hydrogen Storage Materials. *Advanced Materials, 20,* 2105-2110. http://dx.doi.org/ 10.1002/adma.200702605

Jeon, Y. M., Heo, J., & Mirkin, C. A. (2007). Dynamic Interconversion of Amorphous Microparticles and Crystalline Rods in Salen-Based Homochiral Infinite Coordination Polymers. *Journal of the American Chemical Society, 129,* 7480-7481. http://dx.doi.org/10.1021/ja071046w

Jung, S., & Oh, M. (2008). Monitoring Shape Transformation from Nanowires to Nanocubes and

Size-Controlled Formation of Coordination Polymer Particles. *Angewandte Chemie International Edition*, *47*, 2049-2051. http://dx.doi.org/ 10.1002/anie.200704209

Karlin, K. D., & Hogarth, G. (2005). Transition Metal Dithiocarbamates: 1978–2003. *Progress in Inorganic Chemistry, 53*, 71-561. http://dx.doi.org/10.1002/0471725587 .ch2

Kross, R. D., Fassel, V. A., & Margoshes, M. (1956). The Infrared Spectra of Aromatic Compounds. II. Evidence Concerning the Interaction of π-Electrons and σ-Bond Orbitals in C-H Out-of-plane Bending Vibrations. *Journal of the American Chemical Society, 78*, 1332-1335. http://dx.doi.org/10.1021/ja01588a019

Lu, W., Chui, S. S. Y., Ng, K. M., & Che, C. M. (2008). A Submicrometer Wire-to-Wheel Metamorphism of Hybrid Tridentate Cyclometalated Platinum(II) Complexes. *Angewandte Chemie International Edition*, *47*, 4568-4572. http://dx.doi.org/10.1002/ anie.200704450

Lu, W., Chui, S. S. Y.,Ng, K. M., & Che, C. M. (2008). A Submicrometer Wire-to-Wheel Metamorphism of Hybrid Tridentate Cyclometalated Platinum(II) Complexes. *Angewandte Chemie International Edition, 47*, 4568–4572. http://dx.doi.org/10.1002/ anie.200704450

Luo, J., Lei, T., Wang, L., Ma, Y., Cao, Y., Wang, J., & Pei, J. (2009). Highly Fluorescent Rigid Supramolecular Polymeric Nanowires Constructed Through Multiple Hydrogen Bonds. *Journal of the American Chemical Society, 131*, 2076-2077. http://dx.doi.org/10.1021/ja8090774

Mitsumi, M., Murase, T., Kishida, H., Yoshinari, T., Ozawa, Y., Toriumi, K., Sonoyama, T., Kitagawa, H., & Mitani, T. (2001). Metallic Behavior and Periodical Valence Ordering in a MMX Chain Compound, $Pt_2(EtCS_2)_4I$. *Journal of the American Chemical Society*, *123*, 11179-11192. http://dx.doi.org/10.1021/ja010900v

Mueller, H., & Ueba, Y. (1995). A facile synthesis of bis(ethylenedithio)tetrathiafulvalene and related donors for synthetic metals. *Synthetic Metals, 70*, 1181-1182. http://dx.doi.org/10.1016/0379-6779(94)02811-C

Nishiyabu, R., Aime, C., Gondo, R., Noguchi, T., & Kimizuka, N. (2009). Confining Molecules within Aqueous Coordination Nanoparticles by Adaptive Molecular Self-Assembly. *Angewandte Chemie International Edition, 48*, 9465-9468. http://dx.doi.org/10.1002/anie.200904124

Nunez, C., Bastida, R., Lezama, L., Mac ís, A., Perez-Lourido, P., & Valencia, L. (2011). Dinuclear Cobalt(II) and Copper(II) Complexes with a $Py_2N_4S_2$ Macrocyclic Ligand. *Inorganic Chemistry, 50*, 5596-5604. http://dx.doi.org/10.1021/ic200287f

Oh, M., & Mirkin, C. A. (2005). Chemically tailorable colloidal particles from infinite coordination polymers. *Nature, 438*, 651-654. http://dx.doi.org/10.1038/ nature04191

Pandey, R., Kumar, P., Singh, A. K., Shahid, M., Li, P-Z., Singh, S. K., Xu, Q., Misra, A., & Pandey, D. S. (2011). Fluorescent Zinc(II) Complex Exhibiting "On-Off-On" Switching Toward Cu^{2+} and Ag^+ Ions. *Inorganic Chemistry, 50*, 3189-3197. http://dx.doi.org/10.1021/ic1018086

Park, K. H., Jang, K., Son, S. U., & Sweigart, D. A. (2006). Self-Supported Organometallic Rhodium Quinonoid Nanocatalysts for Stereoselective Polymerization of Phenylacetylene. *Journal of the American Chemical Society*, 128 8740-8741. http://dx.doi.org/10.1021/ja062907o

Pavia, D. L., Lampman, G. L., Kriz, G. S., & Vyvyan, J. R. (2007). Introduction Of Spectroscopy, *Cengage Learning* (pp. 22-92).

Peng, A-D., Xiao, D-B., Ma, Y., Yang, W-S., & Yao, J-N. (2005). Tunable Emission from Doped 1,3,5-Triphenyl-2-pyrazoline Organic Nanoparticles. *Advanced Materials, 17*, 2070-2073. http://dx.doi.org/10.1002/adma.200401989

Raja, D. S., Bhuvanesh, N. S. P., & Natarajan, K. (2012). A novel water soluble ligand bridged cobalt(II) coordination polymer of 2-oxo-1,2-dihydroquinoline-3-carbaldehyde (isonicotinic) hydrazone: evaluation of the DNA binding, protein interaction, radical scavenging and anticancer activity. *Dalton Transactions, 41*, 4365-4377. http://dx.doi.org/10.1039/C2DT12274J

Rieter, W. J., Pott, K. M., Taylor, K. M. L., & Lin, W.B. (2008). Nanoscale Coordination Polymers for Platinum-Based Anticancer Drug Delivery. *Journal of the American Chemical Society, 130*, 11584-11585. http://dx.doi.org/10.1021/ ja803383k

Rieter, W. J., Taylor, K. M. L., & Lin, W. (2007). Surface Modification and Functionalization of Nanoscale Metal-Organic Frameworks for Controlled Release and Luminescence Sensing. *Journal of the American Chemical Society,129*, 9852-9853. http://dx.doi.org/10.1021/ja073506r

Rieter, W. J., Taylor, K. M. L., An, H., Lin, W., & Lin, W. (2006). Nanoscale Metal−Organic Frameworks as Potential Multimodal Contrast Enhancing Agents. *Journal of the American Chemical Society*, *128*, 9024-9025. http://dx.doi.org/10.1021/ ja0627444

Sreedaran, S., Bharathi, K. S., Rahiman, A. K., Jagadish, L., Kaviyarasan, V., & Narayanan, V. (2008). Novel unsymmetrical macrocyclic dicompartmental binuclear copper(II) complexes bearing 4- and 6-coordination sites: Electrochemical, magnetic, catalytic and antimicrobial studies. *Polyhedron, 27,* 2931-2938. http://dx.doi.org/ 10.1016/j.poly.2008.06.025

Sun, X., Dong, S., & Wang, E. (2005). Coordination-Induced Formation of Submicrometer-Scale, Monodisperse, Spherical Colloids of Organic−Inorganic Hybrid Materials at Room Temperature. *Journal of the American Chemical Society*, *127,* 13102-13103. http://dx.doi.org/10.1021/ja0534809

Tabata, H., Tokoyama, H., Yamakado, H., & Okuno, T. (2012). Preparation and properties of two-legged ladder polymers based on polydiacetylenes. *Journal of Material Chemistry, 22,* 115-122. http://dx.doi.org/10.1039/C1JM13896K

Tanaka, D., Henke, A., Albrecht, K., Moeller, M., Nakagawa, K., Kitagawa, S., Groll, J. (2010). Rapid preparation of flexible porous coordination polymer nanocrystals with accelerated guest adsorption kinetics. *Nature Chemistry, 2,* 410-416. http://dx.doi.org/10.1038/NCHEM.627

Taylor, K. M. L., Jin, A., & Lin, W. (2008). Surfactant-Assisted Synthesis of Nanoscale Gadolinium Metal–Organic Frameworks for Potential Multimodal Imaging. *Angewandte Chemie International Edition*, 47, 7722-7725. http://dx.doi.org/10.1002/ anie.200802911

West, D. X., Stark, A. M., Bain, G. A., & Leberta, A. E. (1996). Copper(II) complexes of 2-formyl-, 6-methyl-2-formyl-   and 2-benzoylpyridine**N**(4)-(2-methylpyridinyl)-,**N**(4)-(2-ethylpyridinyl)-and **N**(4)-methyl(2-ethylpyridinyl)-thi osemicarbazones. *Transition Metal Chemistry, 21,* 289-295. http://dx.doi.org/ 10.1007/BF00139020

Wohlgemuth, S.-A., White, R. J., Willinger, M.-G., Titirici, M. –M., & Antonietti, M. (2012). A one-pot hydrothermal synthesis of tunable dual heteroatom-doped carbon microspheres. *Green Chemistry, 14,* 1515-1523. http://dx.doi.org/10.1039/ C2GC16415A

Wrochem, F. V., Gao, D., Scholz, F., Nothofer, H. G., Nelles, G., & Wessels, J. M. (2010). Efficient electronic coupling and improved stability with dithiocarbamate-based molecular junctions. *Nature Nanotechnology, 5,* 618-624. http://dx.doi.org/ 10.1038/nnano.2010.119

Yang, D. –Q., Sun, Y., Guo, Y., & Da, D. –A. (1999). X-ray photoelectron spectroscopy of nickel dithiolene complex Langmuir–Blodgett films. *Applied Surface Science, 148,* 196-204. http://dx.doi.org/10.1016/S0169-4332(99)00145-2

Zakirov, A. S., Yuldashev, S. U., Wang, H. J., Lee, J. C., Kang, T. W., & Mamadalimov, A. T. (2011). Study on electrical transport and photoconductivity in iodine-doped cellulose fibers. *Journal of Materials Science, 46,* 896-901. http://dx.doi.org/10.1007/s10853-010-4832-6

Zhang, Z., Chen, K., & Loh, K.P. (2009). Coordination-Assisted Assembly of 1-D Nanostructured Light-Harvesting Antenna. *Journal of the American Chemical Society, 131,* 7210-7211. http://dx.doi.org/10.1021/ja901041d

Zhao, Y., Zhang, J., Han, B., Song, J., Li, J., & Wang, Q. (2011). Metal–Organic Framework Nanospheres with Well-Ordered Mesopores Synthesized in an Ionic Liquid/CO_2/Surfactant System. *Angewandte Chemie International Edition*, *50,* 636-639. http://dx.doi.org/10.1002/anie.201005314

Copyrights